

Multifunctional PMMA-Ceramic composites as structural dielectrics

Eduard A. Stefanescu, Xiaoli Tan, Zhiqun Lin, Nicola Bowler, Michael R. Kessler*

Department of Materials Science and Engineering, Iowa State University, 2220 Hoover Hall, Ames, IA 50011, United States

ARTICLE INFO

Article history:

Received 6 August 2010
 Received in revised form
 9 September 2010
 Accepted 12 September 2010
 Available online 18 September 2010

Keywords:

Nanocomposite
 Polymer
 Ceramic

ABSTRACT

We describe the influence of calcium copper titanate (CCTO), and montmorillonite (MMT) on the thermo-mechanical and dielectric properties of poly(methyl methacrylate) PMMA-based composites prepared by an in-situ, thermally activated, radical polymerization for multifunctional structural capacitor applications. MMT was used for its ability to disperse and suspend the CCTO particles through the generation of viscous monomer slurries. X-ray diffraction (XRD) measurements together with transmission electron microscopy (TEM) analysis revealed that the MMT platelets were present in both intercalated and exfoliated morphologies within the polymer matrix. The filler addition was found to improve the thermal stability and the glass transition temperature of PMMA in the composites. Furthermore, the elastic stiffness and dielectric constant of the resultant composites were observed to increase monotonically with filler loading. By contrast, the dielectric breakdown strength of the composite samples was found to diminish with increasing filler loading.

© 2010 Elsevier Ltd. All rights reserved.

1. Introduction

The increasing demand for energy storage in a wide variety of emerging hybrid vehicles and aircraft has generated considerable effort toward new alternatives for performance, weight and volume improvements in batteries and capacitors [1–4]. The majority of electronic components of various devices are passive, accounting for more than 80% of printed wired surface area [1]. Furthermore, capacitors, especially those with high capacitances, are among the largest passive electronic components. General-purpose ceramic capacitors are mainly used where small sizes along with high capacitances and insulation resistances are required [2]. They are not intended for precision applications due to high variations in the capacitance with temperature. On the other hand, polymer film capacitors are predominantly used in applications requiring low dielectric absorption and loss factors over a wide temperature range [2]. However, polymer film capacitors are characterized by smaller capacitances, due to lower dielectric constants than their ceramic counterparts. It is well known that polymer composites obtained through the addition of ceramic powders into polymeric matrixes, can result in improved dielectric candidates for capacitors with an enlarged spectrum of applications. The spectrum of applications can be even further expanded to structural components when such capacitors are designed with structural characteristics, such as high-strength and stiffness.

Poly(methyl methacrylate), PMMA, is a high-strength, amorphous polymer possessing good dimensional stability and outdoor wearing properties. Owing to these characteristics, PMMA is one of the most heavily studied polymers for nano- and micro-composite fabrications [5–14]. Various in-situ [5,7,8,10,11] and/or ex-situ [9–11,14] approaches have been used to disperse different fillers in PMMA matrixes. Because of its high optical transparency PMMA is commonly employed in various applications as a low-density and shatter-resistant alternative to glass. Additionally, the high stiffness of PMMA, along with its biocompatibility, renders this polymer the matrix of choice in cements for bone-substitute applications [15,16]. Despite its exceptional mechanical behavior, PMMA exhibits a rather low dielectric constant, with values between 3 and 8, depending on molecular weight and testing frequency [10,13,17].

Montmorillonite (MMT) is a well known filler, often used as a reinforcing agent due to its exceptional ability to exfoliate and disperse within polymer matrixes such as PMMA [8,11,12,14]. Smectites such as MMT are 2:1 charged phyllosilicates that contain exchangeable interlayer cations. The 2:1 structure indicates that one octahedral layer of atoms, typically consisting of aluminum, oxygen and hydrogen, is sandwiched between two tetrahedral layers of silicon oxides. The MMT platelets, normally ranging from 60 nm to several hundred nanometers across and 1 nm in thickness, produce an opaque suspension when dispersed in polymer solutions or in monomers such as methyl methacrylate (MMA) [7,11]. Addition of MMT platelets to various polymers have been observed to improve the thermo-mechanical characteristics of the composites [18]. In solution, the polymer and clay build a network-

* Corresponding author. Tel.: +1 515 294 3101.

E-mail address: mkessler@iastate.edu (M.R. Kessler).

like structure, which is interpenetrated by a sub-network of inter-connecting pores containing excess polymer and solvent [19].

Calcium copper titanate, $\text{CaCu}_3\text{Ti}_4\text{O}_{12}$ (here abbreviated CCTO), is a cubic perovskite-related material that has been shown to exhibit a near room temperature effective permittivity of approximately 10,000 [20]. Such a large permittivity strongly suggests that CCTO is a valuable candidate for capacitor-based applications. Although this high permittivity of CCTO has been only recently discovered, [21] the ceramic material has already been used in conjunction with several polymers, such as polystyrene, [22] polyaniline, [23] polyethersulfone, [24] polyvinylidene fluoride, [25] and epoxy resins [26]. Despite this high permittivity, variations in the dielectric behavior of CCTO have been previously observed, even for materials prepared via identical approaches. It has been suggested that such differences may come from intrinsic defects caused by stoichiometry issues, atom vacancies and/or aliovalences of Ti and Cu ions [27]. For this reason, it is important to prepare and compare the behavior of polymer-composite samples containing CCTO filler obtained in one unique batch, as described in this work.

Herein we investigate the effect of CCTO on the thermo-mechanical and dielectric properties of PMMA composites containing MMT. A series of PMMA–MMT–CCTO ternary composites was prepared by effectively dispersing the inorganic nanofiller in organic PMMA-matrix via a thermally-initiated in-situ free-radical polymerization. While CCTO was added to enhance the dielectric constant and energy density of the systems, MMT was added for its thickening ability to help disperse and suspend the CCTO particles. The significant role played by MMT in dispersing and suspending the filler within a methyl methacrylate precursor is demonstrated in Fig. 1. PMMA was the matrix of choice in our composites specifically for its superior mechanical properties and relatively high glass transition temperature. Polymers like polyethylene and polypropylene, heavily employed in the capacitor industry, do not possess the requisite structural characteristics needed in multi-functional capacitors, mainly due to their low glass transition temperatures arising from their substantial chain flexibility. In addition, the dielectric constants and dissipation factors exhibited

by PMMA are very close to those exhibited by polyethylene and polypropylene.

2. Experimental

2.1. Materials

The methyl methacrylate, MMA, monomer (99%, stabilized) used in this work was obtained from Acros Organics. The radical initiator, benzoyl peroxide, BPO, (97% dry weight) was purchased from Alfa Aesar. The montmorillonite, MMT, clay (Cloisite 20A) was provided by Southern Clay Products (Gonzales, TX, USA). Cloisite 20A is Na–MMT modified with dimethyl dehydrogenated tallow ammonium, which imparts hydrophobicity and increases the inter-platelet *d*-spacing. The CaCO_3 (99.95% metal basis), CuO (99.7% metal basis) and TiO_2 (99.8% metal basis) powders, used to prepare the CCTO filler, were purchased from Alfa Aesar.

2.2. Preparation of CCTO

The $\text{CaCu}_3\text{Ti}_4\text{O}_{12}$ powder was prepared by a solid state reaction method. Stoichiometric amounts of CaCO_3 , CuO, and TiO_2 were mixed with vibratory mill in ethanol for 5 h. The dried powder mixture was then calcined at 1000 °C for 12 h. Subsequently, the calcined powder was reground for 5 h to reduce the particle size. Finally, the powder was sieved through a 400 mesh prior to composite fabrication. An X-ray diffraction measurement was conducted from which formation of single phase perovskite-like compound was confirmed. Optical microscopy measurements (see [Supplementary Information](#)) revealed that most CCTO particles have diameters between 1 and 3 μm .

2.3. Preparation of nanocomposites

In order to remove the stabilizing inhibitor from MMA, the monomer was washed three times with a 10% NaOH aqueous solution, followed by three washes with distilled water. The cleaned

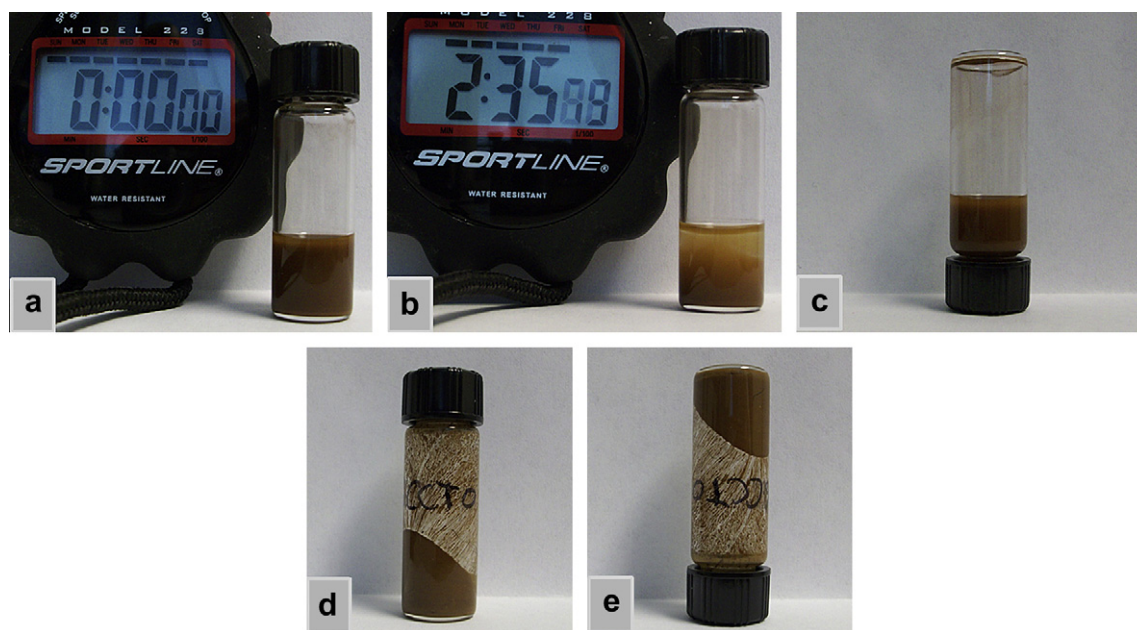


Fig. 1. In a well dispersed MMA–CCTO system a) the CCTO particles begin to sink after as little as 2 min and 35 s b). If the vial is inverted the system immediately flows, being a low-viscosity fluid dispersion c). Addition of MMT to the MMA–CCTO system leads to the formation of a high-viscosity self-supporting gel d) evidenced by the fact that the MMA–MMT–CCTO dispersion does not flow when the vial is inverted e). In d) & e) the dispersive state can be successfully maintained for several days.

monomer was dried using molecular sieves. The molar ratio MMA: BPO was maintained at 1: (2×10^{-3}) by weight in all systems. The first step in the composite preparation was the dissolution of initiator in the monomer, followed by the addition of the thickening agent, MMT, and the second filler, CCTO. The ratio MMA: MMT was maintained constant at 10: 1 by weight in all systems. The systems were then sonicated and mixed at 1–2 min intervals employing a horn sonicator. Subsequently, the systems were centrifuged for approximately 1 min to remove possible air bubbles. The sequence of sonication, mixing and centrifugation was repeated five times for each sample. The in-situ polymerization of all systems was carried out in an oven at 80 °C overnight. Following this procedure, a series of PMMA–MMT–CCTO ternary nanocomposites was prepared. Two reference samples, one PMMA only, and one containing PMMA–MMT, were also prepared for comparison. Gel permeation chromatography (GPC) measurements revealed that the neat PMMA obtained through this method has a molecular weight $MW \approx 770,000$ g/mol and a polydispersity index $PDI \approx 3$. The composition of each sample is described in Table 1.

2.4. Characterization of nanocomposites

Dielectric properties of the samples were characterized using a Novocontrol dielectric spectrometer. Frequency sweeps were performed from 1 Hz to 1 MHz. The dielectric constant and $\tan\delta$ values were recorded with the WinDeta software. Thermogravimetric analysis (TGA) was performed on a TA Instruments Q50 thermobalance. All samples were subject to TGA measurements in air at a heating rate of 20 °C/min. Differential scanning calorimetry (DSC) measurements were conducted using a TA Instruments Q20 analyzer at a heating rate of 10 °C/min. Finally, dynamic mechanical analysis (DMA) was performed using a TA Instruments Q800 analyzer at a heating rate of 3 °C/min. Dielectric breakdown measurements were performed on a CEAST dielectric rigidity apparatus at a frequency of 50–60 Hz, a voltage ramp rate of 0.1 kV/s and a current intensity of 10 mA. Transmission electron microscopy (TEM) was performed using a JEOL 2100,200 kV microscope. The samples were prepared for imaging by ultramicrotomy. Multiple sectioned areas were examined by TEM and only representative images are presented here. Duplicate measurements showed excellent reproducibility of all measured parameters.

3. Results and discussion

3.1. Structure and morphology analysis

Fig. 2a presents the XRD patterns obtained from the PMMA–MMT (10-to-1) composite and from neat PMMA and neat MMT control samples. The range of 2θ angles (1.5° – 7°) presented here was chosen to allow the visualization of the peaks corresponding to the spacing between neat and polymer-intercalated clay platelets. The d -spacing was calculated with Bragg's law ($n\lambda = 2d \times \sin\theta$) for an integer value of $n = 1$. In this relation λ is the

wavelength of the X-rays ($\lambda = 1.54 \text{ \AA}$) and θ is the angle of incidence of X-rays. In the presence of polymer the d -spacing between the MMT platelets increases from 24.2 Å (for the neat MMT) to 38.8 Å, suggesting the existence of polymer-clay intercalated domains. The d -spacing from our analysis for the neat clay agrees exactly with the value provided by the vendor, Southern Clay Products, for this type of montmorillonite (Cloisite20A, $d = 24.2 \text{ \AA}$). As expected, the predominantly amorphous PMMA does not show any peaks in XRD for the range of analyzed angles. Fig. 2b compares the XRD patterns obtained from the PMMA–MMT (10-to-1) composite with those from the 75%(PMMA–MMT)–25%CCTO and 50%(PMMA–MMT)–50%CCTO composites. The range of 2θ angles presented here was chosen, to allow the visualization of the polymer-clay intercalation peak (at small angles), and to display the series of peaks coming from the presence of CCTO (at wider angles). It is clear that addition of CCTO decreases the intensity of the polymer-clay intercalation peak ($d = 38.8 \text{ \AA}$), as seen for the 75%(PMMA–MMT)–25%CCTO sample. Additional CCTO further reduces the intensity of the polymer-clay intercalation peak: for the XRD curve corresponding to the 50%(PMMA–MMT)–50%CCTO sample, only the hint of a peak is visible for an angle around 2.2° . At 2θ angles between 30° and 50° , five peaks corresponding to CCTO are observed for the 75%(PMMA–MMT)–25%CCTO and 50%(PMMA–MMT)–50%CCTO samples. The five perovskite-related peaks coming from CCTO were previously attributed, from left to right, to the following crystallographic planes: (220), (013), (222), (321), (400) [28]. As expected, these peaks are entirely absent from the XRD curve of the PMMA–MMT (10-to-1) composite. Fig. 2c, presents an idealized schematic of the interactions present in the PMMA–MMT–CCTO composites discussed here. In this schematic some intercalated regions are visible, where the polymer chains are situated between adjacent clay platelets and the platelets maintain a degree of parallelism with respect to each other. Additionally, some exfoliated regions are also present, where the polymer-covered platelets lose that parallelism and adopt a random orientation with respect to each other.

TEM measurements were performed to verify the size and morphology of CCTO particles, as well as to observe the intercalation and/or exfoliation of clay platelets. Fig. 3a shows a low magnification micrograph obtained from the 50%(PMMA–MMT)–50%CCTO nanocomposite sample. Several irregularly-shaped, undamaged CCTO particles, varying in size from 1 to about 3 μm , are observed at the top of the micrograph as dark regions. Additionally, multiple CCTO fragments are also present as a result of particles being damaged by the diamond blade during microtoming in the sample preparation procedure. The area marked in Fig. 3a was magnified and displayed in Fig. 3b, where regions of polymer-intercalated clay are predominant, but some isolated exfoliated platelets can also be seen. In fact, most of the discrete areas analyzed by TEM from various spots of the sample revealed a mixture of intercalated and exfoliated clay regions. A magnified domain of polymer-intercalated clay is shown in Fig. 3c. In this image, most polymer-intercalated clay platelets are seen from the edge-on position and the spacing between individual platelets is apparent. Above the intercalated clay region in Fig. 3c, the top surface of a few exfoliated platelets is clearly evident. Through comparison of multiple representative images obtained from various areas of the sample, the results confirmed that both fillers, CCTO and MMT, were uniformly dispersed within the PMMA-matrix.

The structure of the resultant composites is a consequence of the ability of MMT, like many other clays, to exfoliate in a solvent (in our case methyl methacrylate, MMA) and self-assemble into a house-of-cards type of structure (resulting from edge-to-edge and edge-to-face attraction of the exfoliated platelets) with very

Table 1
Sample composition.

No.	Sample Name	Composition (grams)		
		MMA	MMT	CCTO
1	PMMA	10	–	–
2	PMMA/MMT	10	1	–
3	75%(PMMA–MMT)–25%CCTO	10	1	3.6
4	64%(PMMA–MMT)–36%CCTO	10	1	6.2
5	56%(PMMA–MMT)–44%CCTO	10	1	8.6
6	50%(PMMA–MMT)–50%CCTO	10	1	11

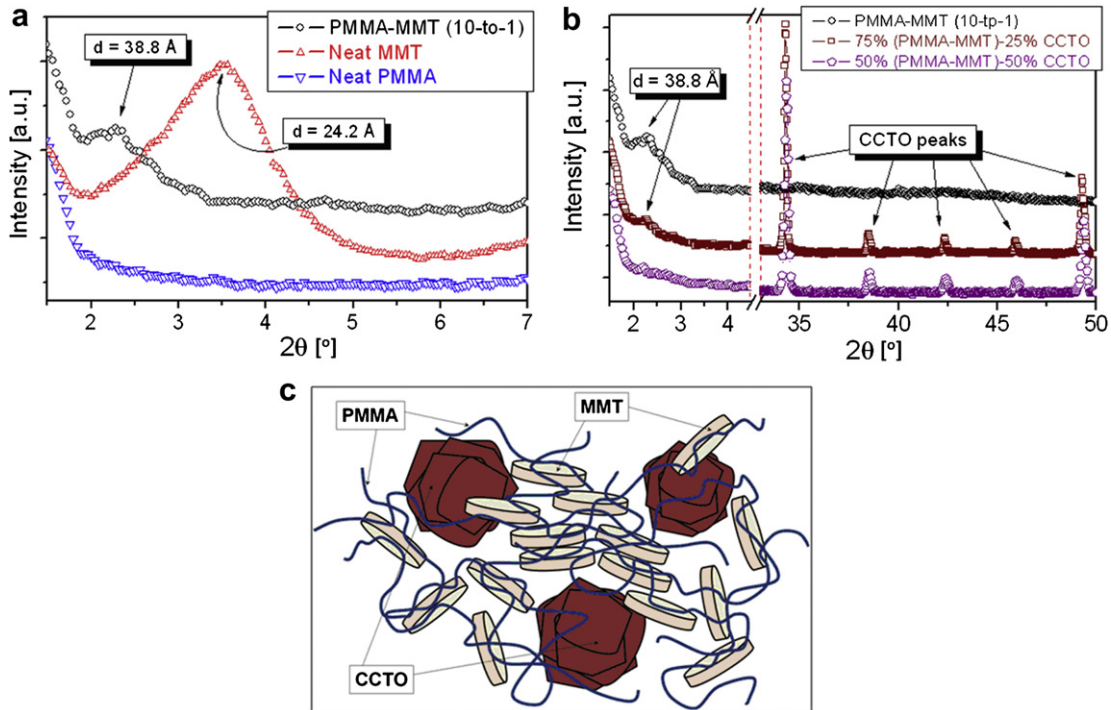


Fig. 2. a) Comparison of the XRD curve of the PMMA–MMT composite with those obtained from the neat PMMA and neat MMT. b) Comparison of the XRD curve of the PMMA–MMT composite with those obtained from the 75%(PMMA–MMT)–25%CCTO and 50%(PMMA–MMT)–50%CCTO composites. c) Schematic describing the coexistence of intercalated and exfoliated domains in CCTO-containing PMMA–MMT composites.

pronounced shear thinning characteristics [29]. Similar effects can be observed when MMT is added to aqueous polymer solutions, where the polymer and the clay build a network-like structure that is interpenetrated by a sub-network of interconnecting pores containing excess polymer and water [30]. The formation of the

house-of-cards network in the presence of clay triggers a tremendous increase in viscosity (compared to the neat methyl methacrylate) which enables the resultant dispersion to behave like a solid in the absence of shear forces. This effect is very well depicted by the illustration in Fig. 1e, where the dispersion does not flow

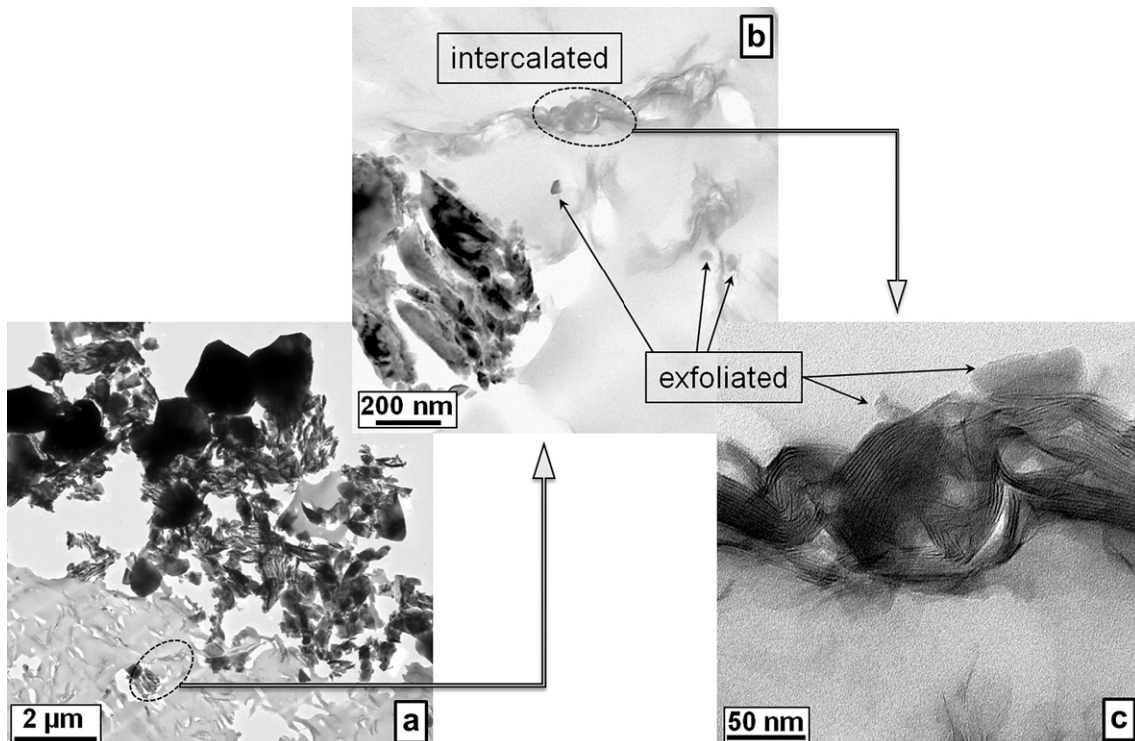


Fig. 3. TEM micrographs obtained from the 50%(PMMA–MMT)–50%CCTO composite sample. Image b) represents a magnification of the area marked in a), and image c) is a magnification of the area marked in b).

following the vial inversion, even after several days. Under these MMT-induced solid-like conditions, the state of dispersion of the CCTO particles, achieved through probe-sonication, is also retained for extended periods, which allows for the MMA polymerization and formation of the composite containing the uniformly dispersed CCTO filler. On the contrary, in the absence of MMT the CCTO particles settle very rapidly to the bottom of the mold when dispersed in the neat MMA monomer (see Fig. 1b).

The combination of XRD and TEM techniques indicated that a mixture of polymer-intercalated and exfoliated nano-sized MMT platelets is present within the PMMA-matrix of all composites. The reduction in the intensity of the MMT intercalation peak with addition of CCTO (see Fig. 2b) might suggest that the micron-sized ceramic filler disrupts the intercalation process and favors the exfoliation of clay platelets. On the other hand, TEM measurements clearly indicated that even in the composite with the highest CCTO loading, 50%(PMMA–MMT)–50%CCTO (see Fig. 3c), polymer-clay intercalated domains are present. A possible reason for the reduction in the intensity of the MMT intercalation peak with addition of CCTO may be the decrease in the MMT weight fraction with increasing the CCTO loading. However, at the highest CCTO loading, 50%(PMMA–MMT)–50%CCTO, the weight fraction of MMT in the composite is approximately 4.6%. Previous studies have shown strong intercalation MMT–PMMA peaks even at clay loadings as low as 3 wt% [7]. For this reason, the dilution effect alone cannot explain the decrease in the intensity of the polymer-clay intercalation peak with increasing the CCTO loading. In light of the TEM findings, we propose that this decrease in the intensity of the MMT–PMMA intercalation peaks with addition of CCTO may be due to an increase in the amount of destructive-interference in the diffraction process during XRD measurements. These destructive-interference effects are mainly attributed to large differences in the d -spacing observed, on one hand for the intercalation of clay platelets ($d = 38.8 \text{ \AA}$), and on the other hand for the crystal structure of the CCTO particles [28]. Additionally, a gradual loss of parallelism of neighboring platelets within intercalated polymer-clay stacked layers may also disrupt the constructively-interfering X-rays that are collected by the detector in the XRD measurements [31]. Such destructive-interference effects have been observed in the past for other polymer-clay systems [31,32].

3.2. Thermo-mechanical analysis

TGA measurements were performed to determine the impact of the filler on the decomposition temperature of PMMA in the resultant composites. TGA and derivative-thermogravimetric (DTGA) data for the PMMA–MMT–CCTO composites and for PMMA and PMMA–MMT reference samples are shown in Fig. 4. From the TGA results it is apparent that addition of the filler increases the decomposition temperature of PMMA. The DTGA analysis (Fig. 4b) reveals two main decomposition peaks for the neat PMMA, at 327 and 382 °C, accompanied by a broad shoulder in between. The DTGA plot also shows that the first decomposition peak observed for neat PMMA is converted into a broad shoulder upon the addition of the fillers, regardless of the CCTO amounts utilized. The addition of MMT to PMMA (PMMA–MMT 10-to-1) shifts the PMMA decomposition peak 20 °C higher than the highest value detected for neat PMMA. Similarly, the decomposition peak values increase when 25% CCTO (by wt.) is added to the composite. However, a slight monotonic decrease of the decomposition temperature is observed with further addition of CCTO in the samples, as indicated by the DTGA measurements (Fig. 4b). The filler residue values (%) from the combustion of the polymeric samples were in a good agreement with the filler amounts weighed during sample preparation.

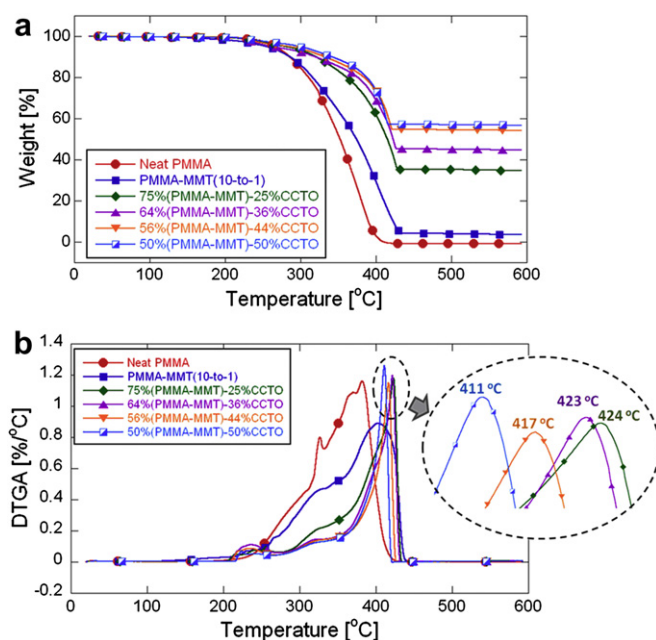


Fig. 4. a) TGA and b) DTGA traces for the PMMA-matrix ternary composites. For comparison, TGA and DTGA traces from reference PMMA and PMMA–MMT samples are also shown. All measurements were performed in air.

Fig. 5a shows the storage modulus (E') and Fig. 5b the loss modulus (E'') of the filled and unfilled polymer samples, as a function of temperature. The DMA curves were obtained from cylindrical bar-shaped samples subjected to a heating cycle with a rate of 3 °C/min at a frequency of 1 Hz. It is clear that all composite

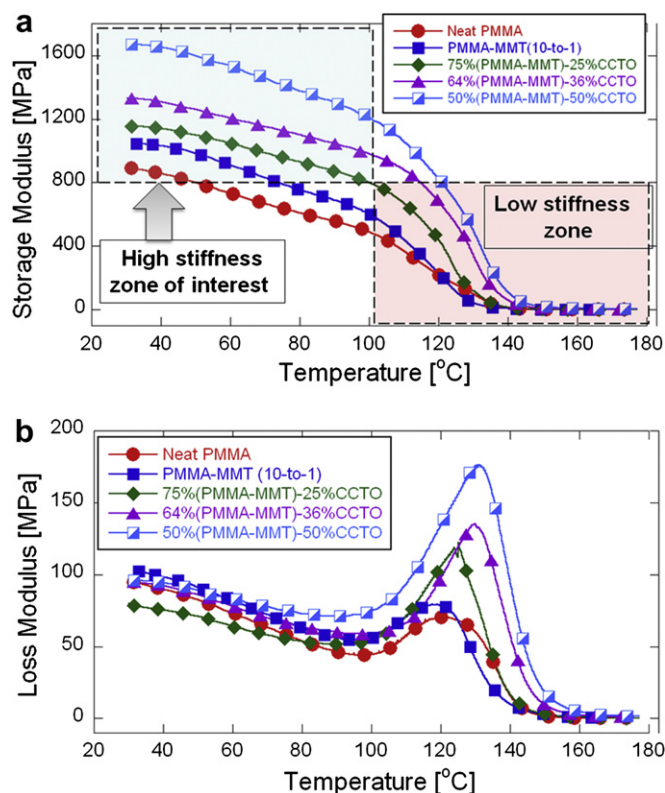


Fig. 5. Storage a) and loss b) modulus for PMMA-matrix ternary composites, reference PMMA and PMMA–MMT samples measured by DMA with heating rate 3 °C/min.

samples exhibit E' values higher than those of neat PMMA. Addition of MMT to PMMA triggers a jump of the E' values. Similarly, addition of CCTO to the PMMA–MMT systems induces a gradual increase of the E' values. As expected, all polymeric samples experience a decrease of the storage modulus at elevated temperatures. The most important features obtained from the E'' curves are the glass transition temperatures (T_g) of the polymeric systems, taken as the temperature where the E'' value is maximum (Fig. 5b). The T_g is observed to increase with addition of the CCTO filler. MMT alone does not seem to positively affect the T_g of PMMA, triggering a slight reduction of the T_g in the PMMA–MMT composite ($T_g = 119$ °C) compared to that of neat PMMA ($T_g = 121$ °C). This feature is highly reproducible. The highest T_g value was observed for the 50%(PMMA–MMT)–50%CCTO ($T_g = 131$ °C).

Improvement in the resistance to degradation of polymers with addition of MMT, or various other fillers is typically attributed to the barrier effect that the fillers provide, as they slow down the volatilization processes of low-molecular weight products from the polymer degradation [10,11]. Consequently, it was not surprising that the temperatures corresponding to the main degradation peaks in the DTGA plot (Fig. 4b) increased from 382 °C for the neat PMMA to 403 °C for PMMA–MMT and to 424 °C for 75% (PMMA–MMT)–25%CCTO. Notably, a decrease in the DTGA-peak degradation temperatures was observed as the CCTO loading was increased in the composites from 25 wt% (424 °C) to 36 wt% (423 °C) to 44 wt% (417 °C) and to 50 wt% (411 °C). This effect indicates that a threshold exists in the composites with respect to the improvement in the degradation stability as a function of filler loading. Similar effects have been observed for other PMMA-ceramic systems, and it has been suggested that at filler loadings higher than a certain limit (dependent on the nature of the filler and/or matrix) the particle-to-particle interactions begin to dominate over the particle-to-matrix interactions that are responsible for degradation-stability enhancements [33]. It is believed that the presence of numerous particles at high loadings perturbs the Van der Waal's interactions between neighboring PMMA chains, thereby affecting the polymer's thermal stability [33]. The three steps that are typically observed when neat PMMA is degraded in N_2 atmosphere, which have been previously attributed to head-to-head linkages, end-chain saturations and random chain scission, [12] cannot be easily detected in the TGA trace obtained from the PMMA degradation in air (Fig. 4). The presence of two peaks and a prominent shoulder between peaks in the neat PMMA DTGA curve, however, suggest that the three distinct processes observed in N_2 atmosphere are also present when the decomposition is conducted in air, where they might occur faster and be partially concomitant.

The increase in the stiffness and T_g of PMMA composites with addition of clays and/or other various ceramic fillers has been observed and reported in the literature [7,14–16]. The increase in the T_g with addition of filler is primarily attributed to a decrease in mobility of the polymer chains owing to the confinement of macromolecules to the filler's surface. Furthermore, the stiffness increase can be primarily attributed to the stiffness of the filler, which in the case of both MMT and CCTO are several orders of magnitude higher than that of the pure polymer. The DMA plot in Fig. 5a has been divided into two main zones taking into account not only the range of desired stiffness, but also the range of temperatures over which composites can be most useful. Although the area designated as “high storage modulus” begins from 800 MPa, for some applications it may be desirable to have modulus values of at least 1 GPa [34]. For the temperature interval lower than 90 °C, all CCTO-containing composites exhibit storage moduli higher than 1 GPa. It is worth noting that many commercial capacitors are rated for temperatures between –50 °C and +80 °C.

For the dielectric composites in the present study, temperatures higher than 80–90 °C would have a negative impact not only on the stiffness of these composites, but also on their dielectric behavior, as will be discussed in the next section. As a final remark, for prototype multilayered structural capacitors, the overall mechanical resistance of the device to the external load-force can be improved not only by elevating the stiffness of each individual dielectric layer, but also by employing a higher number of electrode–dielectric pairs in the multilayered system. That would also result in a higher capacitance of the device, which is desirable in many practical applications.

3.3. Dielectric analysis

The dielectric constant ϵ' and $\tan\delta$ ($\tan\delta = \epsilon''/\epsilon'$) measured at room temperature (25 °C) for the polymeric systems studied here are displayed in Fig. 6a and b, respectively. The dielectric constant of the neat PMMA ($\epsilon' \approx 5$) varied only slightly with frequency, barely decreasing as the frequency was elevated by six orders of magnitude. Addition of MMT increased the dielectric constant of the material to around 7, without changing the frequency dependence trend. At the same time, the dissipation factor trend of the PMMA–MMT remained roughly the same as that of neat PMMA, except for frequencies above 100 KHz. Furthermore, addition of 25 wt% CCTO was observed to double ϵ' values relative to ϵ' of neat PMMA at high frequencies. Following the same trend, ϵ' of the resultant composites increased even more as the CCTO increased to 36, 44 and 50 wt%. The presence of CCTO, however, introduces a larger dependence of ϵ' on frequency. For example, when compared to the ϵ' of neat PMMA at 1 MHz, the ϵ' of the 50% (PMMA–MMT)–50%CCTO composite is 3.5 times larger, but by

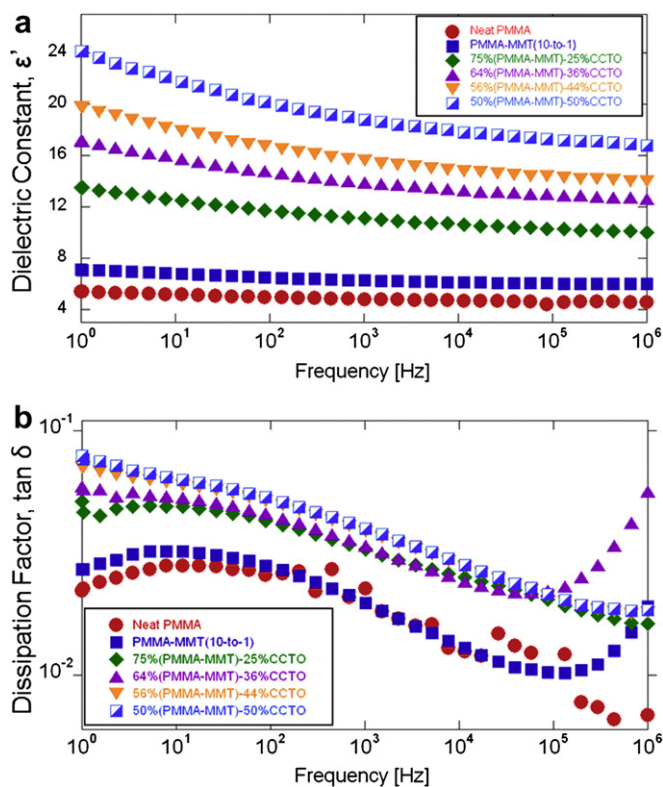


Fig. 6. a) Dielectric constant, ϵ' , and b) dissipation factor, $\tan\delta$, for PMMA-matrix ternary composites, reference PMMA and PMMA-MMT samples measured at room temperature.

contrast at 1 Hz it is close to 4.5 times larger. In addition, the $\tan\delta$ values increase when CCTO is present in the composites. Importantly, $\tan\delta$ of the CCTO-containing composites remains below 10^{-1} for the entire range of frequencies studied.

Fig. 7 shows the temperature-dependent ϵ' and $\tan\delta$ traces for PMMA (a & b) and PMMA–MMT (c & d), respectively, as a function of frequency. The temperature in all measurements was elevated from $-50\text{ }^{\circ}\text{C}$ to $+100\text{ }^{\circ}\text{C}$ in $25\text{ }^{\circ}\text{C}$ increments. For both polymeric systems, higher temperatures resulted in elevated ϵ' and $\tan\delta$ values. For neat PMMA ϵ' and $\tan\delta$ vary only slightly with temperature. For example, at 1 MHz ϵ' increases by less than 0.5 as the temperature increases from $-50\text{ }^{\circ}\text{C}$ to $+100\text{ }^{\circ}\text{C}$, and at 1 Hz the ϵ' increase is approximately 1.6 over the same temperature range. Additionally, for neat PMMA $\tan\delta$ values remain below 10^{-1} for the entire range of frequencies at all temperatures studied. On the other hand, for the PMMA–MMT sample a stronger variation of ϵ' and $\tan\delta$ with temperature is observed, particularly at low frequencies. At 1 MHz, ϵ' increases by less than 0.5 as the temperature is elevated from $-50\text{ }^{\circ}\text{C}$ to $+100\text{ }^{\circ}\text{C}$, whereas at 1 Hz ϵ' increases by more than 20 for the PMMA–MMT composite. Moreover, $\tan\delta$ values of the PMMA–MMT composite stay below 10^{-1} for the entire range of frequencies only at temperatures between $-50\text{ }^{\circ}\text{C}$ and $+50\text{ }^{\circ}\text{C}$. For higher temperatures (e.g. $+75\text{ }^{\circ}\text{C}$ and $+100\text{ }^{\circ}\text{C}$) the $\tan\delta$ remains below 10^{-1} only at high frequencies.

Similar temperature-dependent measurements were performed on the CCTO-containing composites. Fig. 8 shows the temperature-dependent ϵ' and $\tan\delta$ traces for 75%(PMMA–MMT)–25%CCTO (a & b) and 50%(PMMA–MMT)–50%CCTO (c & d), respectively, as a function of frequency. For the CCTO-containing composites, the temperature-induced variation of ϵ' and $\tan\delta$ is even stronger than for the PMMA–MMT composite (Fig. 7). As the temperature is elevated from $-50\text{ }^{\circ}\text{C}$ to $+100\text{ }^{\circ}\text{C}$, at 1 MHz the ϵ'

increases by 0.7 for the 75%(PMMA–MMT)–25%CCTO composite and by 1.5 for the 50%(PMMA–MMT)–50%CCTO composite. At 1 Hz, however, for the same temperature change, ϵ' increases by 37 for the 75%(PMMA–MMT)–25%CCTO composite and by 65 for the 50%(PMMA–MMT)–50%CCTO composite. Increasing the CCTO loadings also leads to an increase of the $\tan\delta$ values and amplifies the $\tan\delta$ change with temperature. At temperatures higher than room temperature $\tan\delta$ remains below 10^{-1} only at high frequencies (10^4 – 10^6 Hz) for the CCTO-containing composites. It should be mentioned that with our measurement setup, dielectric measurements were not possible for samples at temperatures close to, or above, the T_g of the PMMA (ca. $121\text{ }^{\circ}\text{C}$) because of the strong polymer relaxation that results in a change of composite shape and thickness. Such shape and thickness changes in the samples result in an imperfect contact between the metallic electrodes and the polymeric dielectric materials, which induce significant errors in the collected dielectric constant and loss results.

Fig. 9 presents room-temperature dielectric breakdown strength values for the six polymeric systems evaluated at room temperature. Each data point represents the average of three distinct measurements. The breakdown voltage values have been normalized for a thickness of 1 cm to allow comparison of results. An increase in the total amount of filler employed in the composites results in a decrease of the breakdown strength. Addition of MMT to the PMMA (monomer/filler ratio 10/1 – see Table 1) decreases the breakdown strength from approximately 330 kV/cm, for the neat polymer, to around 290 kV/cm. The gradual addition of CCTO to the PMMA–MMT systems decreases the breakdown strength even more, until a final 97 kV/cm value is reached for the 50% (PMMA–MMT)–50%CCTO composite. Additionally, the average diameter of the breakdown area in the tested samples was observed to decrease with increasing amounts of filler (see Supporting

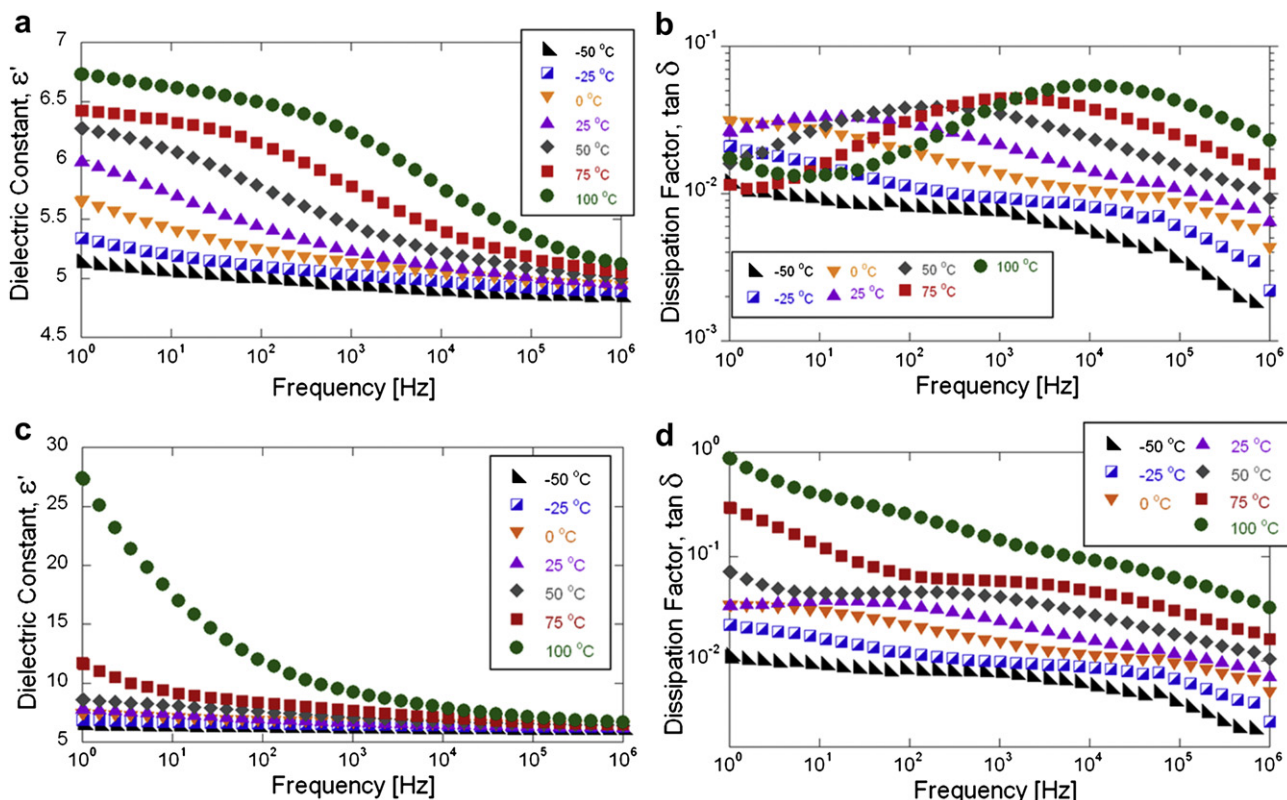


Fig. 7. Dielectric constant and dissipation factor for PMMA (a & b) and PMMA–MMT 10-to-1 (c & d), respectively, as a function of frequency at different temperatures.

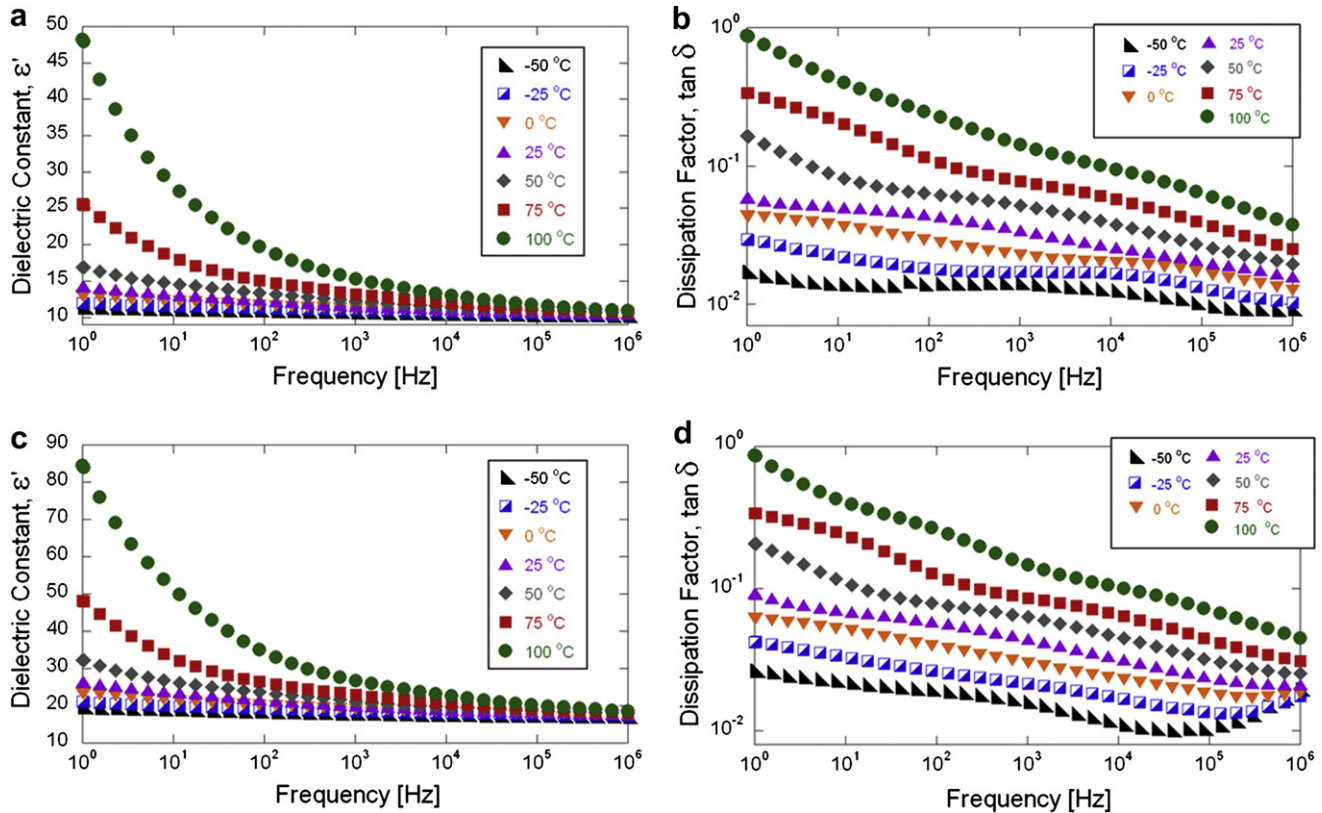


Fig. 8. Dielectric constant and dissipation factor for 75%(PMMA-MMT)-25%CCTO (a & b) and 50%(PMMA-MMT)-50%CCTO (c & d), respectively as a function of frequency at different temperatures.

Information). A linear fitting was performed on the results presented in Fig. 9. The equation obtained from the linear fitting is:

$$Y = 328.74 - 4.205 X$$

in which Y is the breakdown voltage in kV/cm and X is wt.% added filler. The correlation coefficient, R^2 , which shows how well the calculated line fits the original data, is 0.9978, indicating an excellent linear fit. The above relation suggests that breakdown strengths for composites with loadings other than those tested here can be predicted.

It has been previously suggested that the increase of ϵ' at higher filler contents is partially caused by the interfacial polarization effect created between the filler particles, in this case MMT platelets and CCTO, and the polymer [13]. Such interfacial polarization

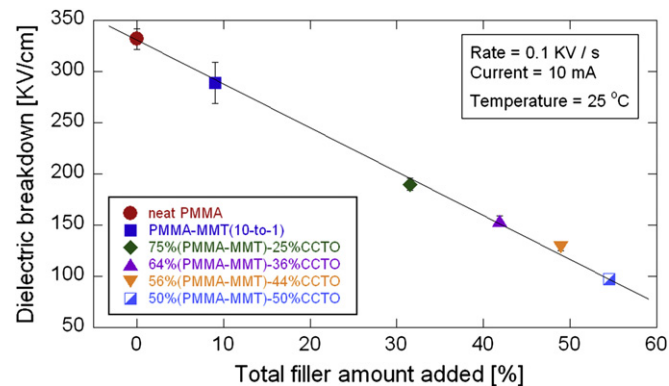


Fig. 9. Dielectric breakdown strength as a function of total filler amount (MMT and CCTO) present in the composites.

effects can occur between MMT platelets, CCTO particles, MMT and CCTO, and/or MMT-CCTO and polymer. Furthermore, at frequencies in the range discussed here, induced atomic, electronic and/or ionic lattice polarizations are essentially instantaneous [13]. Only permanent molecular dipoles, ionic defects of dipolar type and low mobility charge carriers have a non-instantaneous effect that contributes to the overall dielectric loss at these frequencies [35]. The $-\text{COOCH}_3$ groups present on the backbone of the PMMA chains are low mobility dipoles. The permanent molecular dipoles are also present within the CCTO filler, as a result of the uneven distribution of the charge-density between O, Ca, Cu and Ti atoms. In addition, ionic defects can be regularly found in clay platelets such as montmorillonite [19]. It has been also proposed that in dielectric materials one polarization mechanism but lead to a decrease of the dielectric constant. Finally, the dissipation factor decreasing with frequency can be attributed to the inability of the low-mobility charges to follow the applied time-varying field at high frequencies, resulting in a reduction of electronic oscillations. The decrease in the dielectric constant and loss at elevated frequencies is in good agreement with the proposed “universal dielectric response” mechanism [35,36].

Furthermore, the dielectric response of polymer composites at elevated temperatures is affected by several processes including mobility of ionic carriers, and development of space charges and

polarization in the amorphous phase [37]. Upon heating, the combined action of those effects gives rise to an increase of dielectric permittivity of polymers, even in the absence of fillers. However, very small variations of the dielectric constant and dissipation factor with temperature have been reported for pure polymers [2,38]. Similar to the behavior of other polymers, PMMA shows only a minor increase of the dielectric constant with temperature, which is most significant at low frequencies, as indicated in Fig. 7a. The small increase of the PMMA dielectric constant and dissipation factor values with temperature (Fig. 7 a & b) can be attributed to a slight elevation of the dipole moments of the structural repeating units of the polymer with temperature [39]. Additionally, the small dielectric constant and loss values in PMMA, as well as their minor temperature-variations, may also be related to the fact that the rotational conditions regarding the orientations of the polar side groups in the polymer chains are highly restricted, as indicated by differences in the dipole moments of iso-tactic and syndio-tactic PMMA [39]. It has been demonstrated that addition of montmorillonite to polymers, such as poly (vinylidene fluoride), PVDF, amplifies the variation of the dielectric constant with temperature, most likely as a result of an enhanced mobility of ionic carriers at higher temperatures in the presence of clay [37]. Likewise, addition of CCTO to PVDF has been also observed to enlarge the variation of the dielectric constant with temperature, particularly at low frequencies [40]. Similar to what has been observed for PVDF, our results indicate that addition of MMT and CCTO strongly elevates the dielectric constant and dissipation factor values at high temperatures, especially at low testing frequencies (Figs. 7 and 8). These results suggest that structural capacitors based on such PMMA–MMT–CCTO composite dielectrics may be useful in high-temperature-variation environments when utilized with high frequency alternating currents (AC), or utilized for direct current (DC) applications, where the continuous nature of current doesn't cause the dipoles in the dielectric to vibrate and undesirably elevate the ion mobility or produce friction-induced effects such as local heating [2]. It is apparent that for low frequency AC currents, such structural multifunctional capacitors might be valuable for use in environments where the temperature varies only slightly (approximately $\pm 10^\circ\text{C}$).

Finally, the decrease of the dielectric strength of composites with increasing filler loading is expected, since the density of ionic carriers and dipole moments increases with addition of MMT and CCTO [13]. Although the dielectric breakdown value of the 50% (PMMA–MMT)–50%CCTO composite (97 kV/cm) is more than 3 times lower than that of neat PMMA (330 kV/cm), it is still high enough to be of practical importance. For example, a capacitor enclosing a dielectric material based on this ternary composite, with a thickness of 50 μm , would have a dielectric breakdown voltage of around 485 V (97 kV \times 50 μm = 485 V).

4. Conclusions

In summary, PMMA–MMT–CCTO ternary composites are potential dielectric candidates for multifunctional capacitors applications. While the main drawback of commercial general-purpose ceramic capacitors is that they are not suitable for precision applications due to high variations in the capacitance with temperature, the major weakness of commercial polymer film capacitors is that they are characterized by small capacitances due to the reduced dielectric constant of the polymeric films. Here, we have demonstrated that polymer-based composites obtained through the addition of ceramic powders, can result in improved dielectric candidates intended for capacitors with an enlarged spectrum of applications employing high frequency AC currents and/or DC currents. Because these dielectric candidates are also designed for

high mechanical strength and stiffness, the spectrum of applications for capacitors utilizing such dielectrics can be even further expanded to carry mechanical load, improving the overall system efficiency. Possible real-life applications of multifunctional capacitors based on such ternary composites may include designing structural capacitive components, such as structural walls, in ground vehicles and aircrafts, components that would have the ability to store electrical energy while carrying mechanical load.

Acknowledgements

This work is supported by NASA (Cooperative Agreement No. NNX09AP70A). The authors thank Malika Jeffries-EL and Jared Mike of ISU for help with the GPC measurements. Special thanks are extended to Dr. Olesya Zhupanska for her support and thoughtful discussion and to Wei Hu for his help with CCTO powder preparation.

Appendix. Supplementary information

Supplementary data related to this article can be found online at doi:10.1016/j.polymer.2010.09.025.

References

- [1] George S, Sebastian MT. *Composites Science and Technology* 2009;69(7–8):1298–302.
- [2] Kaiser CJ. *The capacitor handbook*. Olathe: CJ Publishing; 1995.
- [3] Lavall RL, Borges RS, Calado HDR, Welter C, Trigueiro JPC, Rieumont J, et al. *Journal of Power Sources* 2008;177(2):652–9.
- [4] Zhang Y, Feng H, Wu XB, Wang LZ, Zhang AQ, Xia TC, et al. *International Journal of Hydrogen Energy* 2009;34(11):4889–99.
- [5] Akat H, Tasdelen MA, Prez FD, Yagci Y. *European Polymer Journal* 2008;44(7):1949–54.
- [6] Chen-Yang YW, Lee YK, Chen YT, Wu JC. *Polymer* 2007;48(10):2969–79.
- [7] Dhibar AK, Mallick S, Rath T, Khatua BB. *Journal of Applied Polymer Science* 2009;113(5):3012–8.
- [8] Khatana S, Dhibar AK, Ray SS, Khatua BB. *Macromolecular Chemistry and Physics* 2009;210(13–14):1104–13.
- [9] Kobayashi Y, Kurosawa A, Nagao D, Konno M. *Polymer Engineering & Science* 2009;49(6):1069–75.
- [10] Kumar S, Rath T, Khatua BB, Dhibar AK, Das CK. *Journal of Nanoscience and Nanotechnology* 2009;9(8):4644–55.
- [11] Lin R-Y, Chen B-S, Chen G-L, Wu J-Y, Chiu H-C, Suen S-Y. *Journal of Membrane Science* 2009;326(1):117–29.
- [12] Oral A, Tasdelen MA, Demirel AL, Yagci Y. *Polymer* 2009;50(16):3905–10.
- [13] Singh NL, Shah S, Qureshi A, Singh F, Avasthi DK, Ganesan V. *Polymer Degradation and Stability* 2008;93(6):1088–93.
- [14] Wu T, Xie T, Yang G. *Journal of Applied Polymer Science* 2010;115(5):2773–8.
- [15] Goto K, Hashimoto M, Takadama H, Tamura J, Fujibayashi S, Kawanabe K, et al. *Journal of Materials Science-Materials in Medicine* 2008;19(3):1009–16.
- [16] Boger A, Bisig A, Bohner M, Heini P, Schneider E. *Journal of Biomaterials Science-Polymer Edition* 2008;19(9):1125–42.
- [17] Nasr GM, Ahmed RM. *Modern Physics Letters B* 2010;24(9):911–9.
- [18] Stefanescu E, Daranga C, Stefanescu C. *Materials* 2009;2(4):2095–153.
- [19] Stefanescu EA, Dundigalla A, Ferreiro V, Loizou E, Porcar L, Negulescu I, et al. *Physical Chemistry Chemical Physics* 2006;8(14):1739–46.
- [20] Ferrarelli MC, Sinclair DC, West AR, Dabkowska HA, Dabkowski A, Luke GM. *Journal of Materials Chemistry* 2009;19(33):5916–9.
- [21] Subramanian MA, Li D, Duan N, Reisner BA, Sleight AW. *Journal of Solid State Chemistry* 2000;151(2):323–5.
- [22] Amaral F, Rubinger CPL, Henry F, Costa LC, Valente MA, Barros-Timmons A. *Journal of Non-Crystalline Solids* 2008;354(47–51):5321–2.
- [23] Thomas P, Dwarakanath K, Varma KBR. *Synthetic Metals* 2009;159(19–20):2128–34.
- [24] Wang F, Zhou D, Hu Y. *Physica Status Solidi (a)* 2009;206(11):2632–6.
- [25] Arbatti M, Shan X, Cheng Z-Y. *Advanced Materials* 2007;19(10):1369–72.
- [26] Shri Prakash B, Varma KBR. *Composites Science and Technology* 2007;67(11–12):2363–8.
- [27] Romero JJ, Leret P, Rubio-Marcos F, Quesada A, Fernández JF. *Journal of the European Ceramic Society* 2010;30(3):737–42.
- [28] Ramírez MA, Parra R, Reboredo MM, Varela JA, Castro MS, Ramajo L. *Materials Letters* 2010;64(10):1226–8.
- [29] Das A, Costa FR, Wagenknecht U, Heinrich G. *European Polymer Journal* 2008;44(11):3456–65.
- [30] Stefanescu EA, Petrovan S, Daly WH, Negulescu II. *Macromolecular Materials and Engineering* 2008;293(4):303–9.

- [31] Stefanescu EA, Daly WH, Negulescu II. *Macromolecular Materials and Engineering* 2008;293(8):651–6.
- [32] Stefanescu EA, Stefanescu C, Daly WH, Schmidt G, Negulescu II. *Polymer* 2008;49(17):3785–94.
- [33] Chatterjee A. *Journal of Applied Polymer Science* 2010;116(6):3396–407.
- [34] South JT, Carter RH, Snyder JF, Hilton CD, O'Brien DJ, Wetzel ED. *Materials Research Society Symposium Proceedings* 2005;851. NN4.6.1–NN4.6.11.
- [35] Jonscher AK. *Nature* 1977;267(5613):673–9.
- [36] Ngai KL, Jonscher AK, White CT. *Nature* 1979;277(5693):185–9.
- [37] Kelarakis A, Hayrapetyan S, Ansari S, Fang J, Estevez L, Giannelis EP. *Polymer* 2009;51(2):469–74.
- [38] Venkat N, Dang TD, Bai Z, McNier VK, DeCerbo JN, Tsao B-H, et al. *Materials Science and Engineering: B* 2009;168(1–3):16–21.
- [39] Shima M, Sato M, Atsumi M, Hatada K. *Polymer Journal* 1994;26(5):579–85.
- [40] Thomas P, Varughese KT, Dwarakanath K, Varma KBR. *Composites Science and Technology* 2010;70(3):539–45.